Properties of electrons in bismuth

V. S. Édel'man

Institute of Physics Problems, USSR Academy of Sciences
Usp. Fiz. Nauk **123**, 257–287 (October 1977)

A review is presented of the studies on the basis of which the contemporary model of the carrier spectrum in bismuth has been established. Descriptions are presented of the theoretical models and of experiments that make it possible to elucidate their connection with the real spectrum and with the parameters of the models. These experiments include investigations of the conduction electrons on the Fermi level and measurement of the characteristics of the Fermi surface, magneto-optical investigations of the closely-located valence and conduction bands, and investigations in a quantizing magnetic field. Problems that require further refinement are considered, and experiments that can contribute to progress in this field are proposed.

PACS numbers: 71.25.Hc, 78.20.Ls

CONTENTS

1. Introduction 819
2. Theoretical Premises Concerning the Spectrum of Bismuth 820
3. The Fermi Surface of Bismuth 823
4. Investigations in the Infrared Band 827
5. Investigations of Bismuth in the Quantum Limit 829
6. Spectrum of the Electrons of the Lower Landau Level. 830
7. Hole Spectrum 832
8. Conclusion. 834
References. 834

1. INTRODUCTION

Bismuth attracts constant and unabated attention of solid-state specialists (Fig. 1). This interest is due to its unique electronic properties: low carrier density $\sim 10^{-5}$ electrons/atom; low effective masses $\sim 10^{-2} m_e$ (m_e is the mass of the free electron), large diamagnetic susceptibility $\sim 10^{-5}$, large dielectric constant ~100, and large value of the g factor, which reaches ~200.

Because of these properties, investigations of bismuth have played a special role in metal physics. It suffices to state that bismuth was the substance in which the first observations were made of strong magnetoresistance,[1] of the de Haas–van Alphen effect,[2] of the Shubnikov–de Haas effect,[3] of oscillating magnetostriction,[4] of cyclotron resonance in metals,[5] and of undamped microwaves.[6] The first detailed measurements of the magnetic surface levels[7] and geometric oscillations of ultrasound[8] were also made with this metal. One can state without exaggeration that the study of the foregoing phenomena has been the reason for the progress made so far in metal physics.

The investigation of the electronic properties of bismuth—and it is precisely these properties which make it unique—is of interest because of the intermediate position occupied by bismuth between good metals and semiconductors. Bismuth is a representative of the class of substances whose electronic properties are closely connected with the small deviation of the crystal lattice from a more symmetrical modification.[9] Foremost among them are the semimetals Bi, Sb, and As, and the binary alloys Bi–Sb, which have a rhombohedral close-to-cubic lattice. From among these substances, from the point of view of the experimental investigation, bismuth offers undisputable advantages in that it is easily obtained in the form of a high-grade single crystal with large electron mean free path, as much as ~1 mm. This makes it possible to investigate a large group of physical phenomena and to obtain the parameters of the bismuth spectrum with good accuracy.

The purpose of the present review is to describe the results of the most complete and exact contemporary investigations of the energy spectrum of the electrons in bismuth. As a rule, we shall not pay attention to the historical picture. The reader interested in these questions is advised to turn to the reviews[10,11]. In those

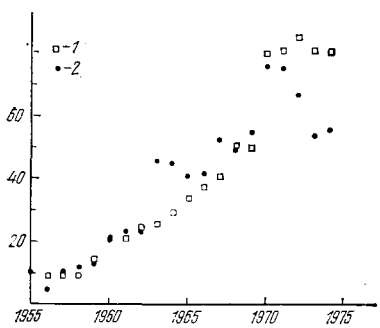

FIG. 1. Number of abstracts of articles on the properties of bismuth and bismuth-antimony alloys, published in "Physics Abstracts," compared with the total number of abstracts. 1—total number of abstracts (in thousands), 2—papers on the electronic properties of bismuth.

 0038-5670/77/2010-0819$01.10

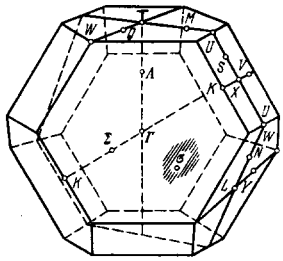

FIG. 2. Brillouin zone of bismuth.

cases when the large number of publications devoted to some particular problem includes one or two papers that overlap the material in the others, we shall present only the results of these comprehensive papers. Comparison with other investigations can be found in the review[12].

2. THEORETICAL PREMISES CONCERNING THE BISMUTH SPECTRUM

a) Calculation of band structure

The first calculations of the band structure of bismuth were performed by Mase,[13] who, taking into account the special role of high-symmetry points, calculated the energy levels along the lines Γ–T and Γ–L of the Brillouin zone (Fig. 2). Subsequently, Ferreira[14,15] calculated the energy levels at the points Γ and T (symmetry group D_{3d}) and X and L (group C_{2h}). Calculations by the augmented-plane-wave method, the results of which are given in Table I, has established that the holes are located at the T points and the electrons at the L points of the Brillouin zone. A similar disposition of the regions of the Fermi surface was established earlier by Abrikosov and Fal'kovskiĭ on the basis of the deformation model proposed by them.[9]

A general idea concerning the band structure of bismuth was obtained by Golin by a pseudopotential-method calculation.[16] The accuracy of the calculations by this method, as is well known, usually amounts to 0.5–0.1 eV. The characteristic energies of the electrons and holes in bismuth are ~0.01 eV. An attempt was therefore made in[16] to describe the carriers by choosing the parameters of the pseudopotential in such a way that the overlap of the bands in L and T and the small energy

TABLE I. Energy levels at the points T, Γ, L, and X.

Designation of level*	Energy relative to the Fermi level, eV from[16]	from[14]	Designation of level*	Energy relative to the Fermi level, eV from[16]	from[14]
T_{45}^+	1.57	1.12	Γ_6^-	3.04	3.15
T_6^-	0.89	0.61	Γ_6^-	0.65	1.00
T_6^+	0.52	0.095	Γ_6^+	—0.17	—0.34
T_{45}^-	0.02	0.205	Γ_{45}^+	—0.18	—0.58
T_6^+	—1.58	—1.3	Γ_6^+	—2.45	—2.55
T_6^-	—1.89	—1.68			
L_a	1.51	1.05	X_s	2.07	2.43
L_s	1.10	0.65	X_a	—1.53	—1.98
L_s	—0.019	—0.095	X_a	—3.01	—3.22
L_a	—0.034	—0.335			
L_a	—1.84	—1.40			
L_s	—1.95	—1.68			

*This designation corresponds to Fig. 3.

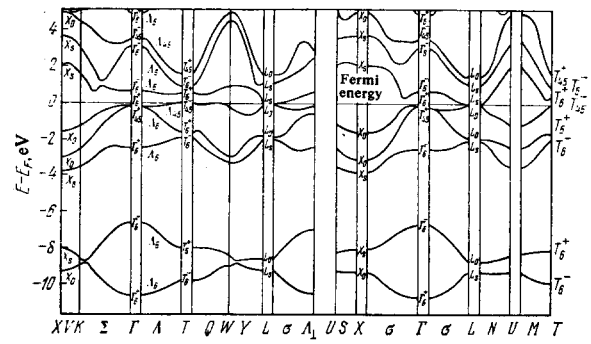

FIG. 3. Band structure according to Golin.

gap between the conduction and valence bands in L (its presence followed from optical investigations—Ch. 4) coincided with the experimental values.[17] The results of Golin's calculations are given in Table I and in Fig. 3. Comparison of the calculations of[15] and[16] (see Table I) with measurements of the optical absorption[18] (Table II) leads to the conclusion that the theory accounts for the band structure with accuracy 0.2–0.4 eV. This conclusion, however, cannot be regarded as final, since the number of lines observed in the optical band is relatively small. At the same time, the band structure is quite complicated (see Fig. 3) and, in principle, the observed singularities can be due to transitions between other levels that are not indicated in Table II.

The $k\pi$ perturbation theory, which makes use of the energy levels and wave functions obtained in the pseudopotential calculation, was employed by Golin to calculate the carrier-mass tensor.[16] It turned out that the mass-tensor components of both the electrons and the holes differed from the measured ones by a factor 2–3. In addition, according to the calculation, the angle of inclination of the electron ellipsoid to the basal plane was +10° and the ratio of the maximum momentum to the minimum momentum was 6. Experiment yields for these quantities +6°23' and 13.9, respectively (see Fig. 4; see also Ch. 3).

Thus, although the calculations by the pseudopotential method[16] and by the augmented-plane-wave (APW) method[15] give a general idea of the band structure, they are not very suitable for the description of the bismuth carriers, which have a characteristic energy (~10^{-2} eV) lower by one order of magnitude than the calculation accuracy. It is of interest, however, to consider the inverse formulation of the problem—use the available experimental data to refine the positions of the energy lev-

TABLE II. Interband-transition energies measured in[18] compared with the calculation by the pseudopotential method.[16]

Energy, eV from[18]	from[16]	Transition between bands	Level designations	Energy, eV from[18]	from[16]	Transition between bands	Level designations
0.69	0.82	5→6	$\Gamma_6^+ \to \Gamma_6^-$	2.96	2.94	4→7	$L_a \to L_s$
0.81	0.83	4→6	$\Gamma_{45}^+ \to \Gamma_6^-$	3.33	3.20	4→7	$\Gamma_{45}^+ \to \Gamma_6^-$
1.15	1.13	5→7	$L_a \to L_s$		3.19	5→7	$\Gamma_6^+ \to \Gamma_6^-$
1.68	1.53	6→8	$L_s \to L_a$		3.41	3→8	$L_s \to L_a$
1.92	1.83	4→6	$L_a \to L_s$	3.57	3.62	4→8	$\Gamma_{45}^+ \to \Gamma_{45}^-$
2.49	2.48	5→7	Near Σ		3.62	5→8	$\Gamma_6^+ \to \Gamma_{45}^-$
	2.51	4→7	Near Λ		3.60	5→6	$X_a \to X_s$

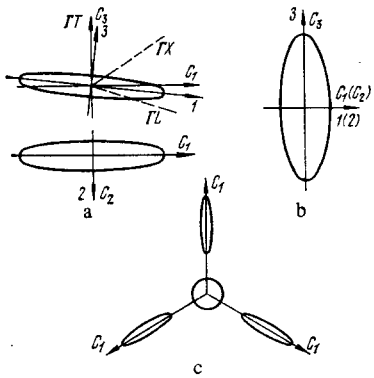

FIG. 4. Diagrams of electron (a) and hole (b) Fermi surfaces, their orientations relative to the crystal lattice and the directions in the Brillouin zone, and the relative placement of the electron and hole surfaces (c).

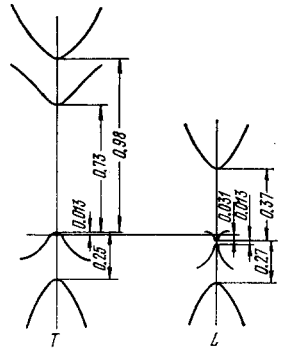

FIG. 5. Band structure of bismuth in the deformation model.[26] The energy differences are in eV.

els at least at the point T, which has the highest symmetry. Although several attempts at this type of calculations are known,[15,16,19,20] the problem cannot be regarded as finally solved. The point is that these studies yielded $\delta E \approx 0.2$ eV for the distance from the valence band, whose position practically coincides with the Fermi level, to the neighboring band. At the same time, in the optical investigations[18,21] at energies 0.1–0.7 eV, no singularities were observed that could be connected with transitions between the bands. On the other hand, we regard it as premature to attribute the anomalies of the current-voltage characteristics, observed in the same energy region in bismuth-insulator-aluminum junctions,[22] to singularities of the band structure, if no other reason that other workers obtained entirely different forms for these characteristics.[23,24]

b) Deformation theory

The deformation theory[9,10] starts from the premise that a real bismuth crystal, which has a rhombohedral lattice with two atoms per unit cell, can be regarded as a result of stretching a primitive cubic lattice along one of the body diagonals and a relative shift of the neighboring phase-centered sublattices along this diagonal. In the initial cubic lattice, in the free-electron approximation, there is a triply degenerate level[1)] whose energy is close to the Fermi energy at points located on threefold axes half way between the center and the face of the Brillouin zone. The crystal field lifts the degeneracy partially and splits off one of the levels. According to a postulate of the theory,[9] the doubly degenerate level (its small splitting is due only to spin-orbit interaction) at this point of the Brillouin zone coincides exactly with the Fermi level and causes the electron and hole Fermi surfaces to coincide.

An infinitesimally small shift of the sublattices double the reciprocal-lattice period. As a result, the considered electron and hole Fermi surfaces become exactly congruent, and the metal turns into a dielectric.[2)] This state with a fourfold degenerate level is the starting point for the construction of the spectrum within the framework of perturbation theory at finite but small rhombohedral deformations and sublattice shift. The spectrum of Abrikosov and Fal'kovskiĭ (Fig. 5) is described by equations of fourth order in the momentum components, and contains seven parameters that are connected with the observed quantities by a complicated relation.[10,26] A consistent comparison of theory with experiment calls for a computer calculation. There is only one known attempt of this type.[26] Fal'kovskiĭ and Razina succeeded in obtaining agreement between the theoretical sections of the Fermi surface and the theoretical effective masses, on the one hand, and experiment, on the other, within ~10–20%. Using the spectrum parameters calculated in[26], Fal'kovskiĭ calculated the spin splitting.[27] The anisotropy of the g factor for the electrons agreed qualitatively with experiment. For holes at $\mathbf{H} \parallel C_3$, the g factors turned out to have half the measured value.

The difference between the theoretical and experimental g factors for holes is of fundamental significance, since it cannot be eliminated by any choice of parameters.[27] Abrikosov[28] calculated the spectrum at the point T with account taken of all six levels referred to at the beginning of this section. He has shown that the effective g factor of the holes[3)] at $\mathbf{H} \parallel C_3$ can be larger than two if the valence band is formed from one of the additional levels not taken into account in the difference variants of the deformation theory. We note also that the addition of two more levels to the scheme shown in Fig. 5 makes it much more similar to the Golin band scheme[16] (see Fig. 3 and Table I).

Some conclusions of the deformation theory, concerning the form of the electron spectrum, will be considered in the next section.

c) Models of electron spectrum

An important role in the investigation of bismuth is played by the models of the electron spectrum. They

[1)] In the absence of a field, each of these levels is additionally doubly degenerate in spin.

[2)] This picture actually takes place for binary alloys of the type PbTe, SnTe and others, which have a cubic lattice.[25]

[3)] The effective g factor is the ratio of double the spin splitting to the cyclotron splitting.

are based on the fact known from optical investigations, that two bands are close at the point L (Ch. 4). Taking into account only these close bands, and using perturbation theory, we obtain the spectrum known as the Lax model

$$\frac{P_i P_k}{m_{ik}} = \frac{[E-(E_g/2)][E+(E_g/2)]}{E_g}, \tag{1}$$

where P_i are the momentum components, m_{ik} is the effective-mass tensor, E_g is the gap between the bands; the energy E is reckoned from the midpoint between the valence and conduction bands. The proximity of the two bands leads, in addition to the smallness of the effective masses, to a large value of the g factor,[30] so that the effective g factor is exactly equal to 2, and the spin splitting is equal to the cyclotron value. Therefore, in a quantizing magnetic field $\mathbf{H} \parallel z$, the spectrum (1) corresponds to energy levels that are determined at $P_z = 0$ by the equation[29,31]

$$E_n = \pm \sqrt{\frac{E_g^2}{4} + E_g\left(n+\frac{1}{2}+s\right)\frac{e\hbar H}{m_0^* c}}, \tag{2}$$

or the equivalent equation

$$\left(E_n - \frac{E_g}{2}\right)\left(E_n + \frac{E_g}{2}\right) = E_g \frac{e\hbar H}{m_0^* c}\left(n+\frac{1}{2}+s\right), \tag{2'}$$

where n is the number of the Landau level, s is the electron spin, m_0^* is the effective mass at the extremum of the band and is of the order of $10^{-2} m_e$ (m_e is the mass of the free electrons); the plus and minus signs pertain to the conduction and valence bands, respectively.

The electron Fermi surface of bismuth is strongly stretched along the 1 axis, which is close to the direction of the bisector axis C_1 (see Fig. 4). It follows hence that the matrix element describing the interaction of two nearest bands in this direction should be smaller by a factor $\sim 10^2$ than for directions perpendicular to the elongation. Cohen[32] advanced the hypothesis that there is no interaction at all in the direction of the 1 axis, and the spectrum is determined by the more remote bands. Calculation within the framework of the effective-mass method leads to the spectrum

$$\left(E - \frac{E_g}{2} - \frac{P_1^2}{2m_{1+}}\right)\left(E + \frac{E_g}{2} + \frac{P_1^2}{2m'_{1-}}\right) = E_g\left(\frac{P_2^2}{2m_2} + \frac{P_3^2}{2m_3}\right). \tag{3}$$

The parameters in this formula are of the order of

$$m_{1+} \approx m_{1-} \approx m_e, \quad m_2 \approx m_3 \approx 10^{-2} m_e, \quad E_g \approx 10 \text{ meV}.$$

The orthogonal coordinate axes are chosen as shown in Fig. 4.

Abrikosov has established[33] that Cohen's spectrum (3) can be obtained from the deformation model if E_g is assumed to be a small quantity. Later on, Beneslavskiĭ and Fal'kovskiĭ[34] have shown that if the spin-orbit coupling is taken into account as a small perturbation, then there exists a direction in which there is no interaction between the nearest bands, and in the two-band model the equal-energy surfaces are cylindrical. By the same token, the reason for the elongation of the Fermi surface can be regarded as established, and Cohen's hypothesis can be regarded as theoretically proven. In light of[34], the existence of the nonquadratic ellipsoidal Lax model (1) seems impossible. Therefore Cohen's model is the principal approximation for the spectrum at $E \approx E_g$ and is just as fundamental as the quadratic spectrum at $E \ll E_g$.

The levels corresponding to the spectrum (3) were calculated in a magnetic field by Baraff[31] for the case when H is parallel to the 1 axis (or is close to it, so long as the spin splitting differs little from the Landau splitting) and $P_z = 0$. The levels were calculated in[34] for arbitrary P_z, but within the framework of a concrete model that takes into account the interaction of only four bands with one another. For the Landau levels, the expression obtained in[34] coincides at $j = n + (1/2) + s \neq 0$, $P_z = 0$ with that given in[31]. For $j = 0$, i.e., for the lower level in the conduction band or the upper level in the valence band, the result obtained in[34] is

$$E = \pm\left(\frac{E_g}{2} + \frac{e\hbar H}{2c}\Delta_\pm - \frac{P_z^2}{2m_{1\pm}}\right), \tag{4}$$

where the upper and lower signs pertain to the conduction and valence bands, respectively. The parameter $\Delta_\pm \approx 10^{-1}/m_{01}^*$ describes the relatively small influence of the remote bands, which leads to a difference between the spin splitting and the Landau splitting (cf. formula (2)). The term proportional to P_z^2 corresponds to a parabolic dependence of the energy on the momentum in the elongation direction in Cohen's model (3).

Baraff,[31] and later Vecchi *et al.*,[21] proposing for the same level a mutual interaction that, generally speaking, should be nonexistent because of the different parities of the valence and conduction bands,[21] obtained a spectrum that takes at $\Delta_+ = -\Delta_- = \Delta$ and $P_z = 0$ the form

$$E = \pm \sqrt{\left(\frac{E_g}{2} + \frac{e\hbar H}{2c}\Delta\right)^2 + \left(\frac{e\hbar H}{c} b\right)^2}, \tag{5}$$

which goes over into the system (4) at $b = 0$. As noted in[21], introduction of the finite value of b is justified by the fact that without allowance for this quantity it is difficult to explain the experiments on magnetoreflection (see Sec. 6 of Ch. 4).

A number of experiments have established that the Fermi surface deviates from Cohen's model (see Ch. 3). Models were therefore considered, in which a large number of perturbation-theory terms were taken into account. Their role turns out to be significant because of the numerical smallness of the matrix elements describing the interaction of the bands in the elongation direction. This manifests itself in the fact that the masses m_{1+} and m'_{1-} in (3) turn out to be of the order of m_e, although they could be also smaller by one order of magnitude, as is observed for Ge or Si, which have an energy gap ~ 1 eV and effective masses $\sim 0.1\, m_e$. The most complete electron-spectrum model, which is a mixture of the Cohen and Lax spectra and supplements them with fourth-order terms of the type $P_1^2 \times P_{2,3}^2$ and $P_1^3 \times P_{2,3}$, was proposed by McClure and Choi.[35] We shall consider it when we discuss the experimental results.

TABLE III.

Direction of H	m_i^*, [a] $10^{-2}\,m_e$	$\lim_{m_i^*}$ $10^{-2}\,m_e$	S_i, [b] 10^{-42} (g-cm/sec)	P_i [c] 10^{-21} g-cm/sec	Curvature radii at the limiting point in 10^{-21} g-cm/sec	v_i, 10^7 cm/sec	Effective g factor [b]*
Electrons, angle between C_1 and the 1 axis is 6°23' ± 1', [b]							
Axis 1	0.82 ± 0.005	0.90 [d]	1.300 ± 0.003	7.88	0.0518 0.104	0.89 [e]	2.18 ± 0.02
Axis 2	11.9 ± 0.05	13.8 ± 0.2 [a]	19.27 ± 0.05	0.559	177 0.983	10.0 [f]	0.5 ± 0.2
Axis 3	8.8 ± 0.2	11.7 ± 0.4 [a]	14.35 ± 0.04	0.740	163 0.422	7.5 [f]	1.06 ± 0.06
Holes							
C_1, C_2	21.2 ± 0.05		22.49 ± 0.02	5.89		8.38 [g]	< 0.1
C_3	6.39 ± 0.03		6.76 ± 0.01	1.772		2.52 [g]	4.26 ± 0.02

[a] Measured in [12,41,54]. [b] Measured in [27]. [c] Calculated from the results of [37]. P_i is accurate to ≈ 0.2% and the curvature radii to ≈ 1%. [d] Calculated from the curvature radii and the velocity. [e,f] Calculated from the curvature radii and the results of measurements of the resonance of the magnetic surface levels in [60] [e] and [58] [f]; accuracy ~ 3% [e] and ~ 1% [f]. [g] Calculated for the ellipsoidal model; accuracy ~ 0.5%.

*The minimum value of the g factor is 0.70 ± 0.4 in the binary plane and is observed at an angle 3.5° between H and C_3.

3. THE FERMI SURFACE OF BISMUTH

At the present time there are many known experimental methods with which to establish the shape of the Fermi surface of metals and the carrier velocities on these surfaces. These include the following: investigation of the quantum oscillations of the magnetic moment or of the conductivity, etc., geometrical size effects, size and resonant oscillations of ultrasound damping, galvanomagnetic investigations, study of magnetoplasma waves, cyclotron resonance, and observation of the magnetic surface levels. All these methods were used to investigate the electronic properties of bismuth. As a result, a well known model of the Fermi surface has by now been established, consisting of three strongly elongated electronic sections, close in shape to ellipsoids, and a hole ellipsoid of revolution (see Fig. 4).[10] We consider below in greater detail the experiments which at the present time yield the most exact information on the Fermi surface of bismuth.

a) Quantum oscillations of the conductivity. Shape of the electron Fermi surface

It is well known that at low temperatures the thermodynamic potential oscillates when the magnetic field is varied,[36] and this leads to quantum oscillations of the magnetic moment, of the conductivity, etc. The period of these oscillations in terms of the reciprocal magnetic field is

$$\Delta H^{-1} = \frac{ch}{S}, \qquad (6)$$

where S is the area of the extremal section of the Fermi surface. As the temperature T and the Dingle temperature T_D (which characterizes the broadening of the Landau levels as a result of the crystal defects) decrease, the quantum oscillations acquire in strong fields the form of peaks with relative width $\sim k(T+T_D)/\hbar\Omega$, and the region in which they can be observed extends in a weak field to $H \sim k(T+T_D)m^*c/\hbar e$ (m^* is the effective mass). Accordingly, the measurement accuracy increases in proportion to the decrease of $(T+T_D)$.

The smallest value $T_D + T \approx 0.2$ °K was attained in [37], where the sections of the Fermi surface were measured in the trigonal and binary planes accurate to ~ 0.2–0.3% (Table III, Fig. 6) and the spin splitting was measured accurate to ~ 1% (Table III and Fig. 7). The results obtained in other papers devoted to the investigation of the de Haas–van Alphen or the Shubnikov–de Haas effects agree with the results of [37] within the limits of measurement errors of these studies, ~ 1–10%. The anisotropy of the cross sections is described in first-order approximation by an ellipsoidal Fermi surface

$$\frac{P_1^2}{P_{10}^2} + \frac{P_2^2}{P_{20}^2} + \frac{P_3^2}{P_{30}^2} = 1,$$

where the subscripts 1, 2, and 3 pertain to the principal axes of the ellipsoid (see Fig. 4). The 1 axis lies

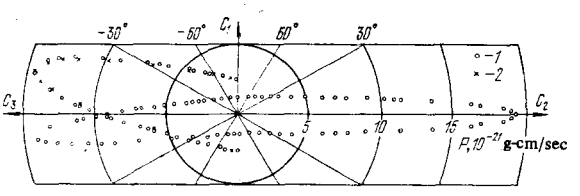

FIG. 6. Anisotropy of the extremal sections in the trigonal and binary planes: 1—experiment, 2—ellipsoid.

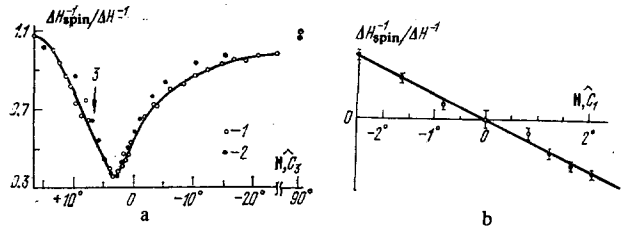

FIG. 7. Anisotropy of relative spin splitting in binary planes for electrons (a) and holes near the bisector axis (b): 1—measured in[37], 2—calculated from data of[17].

in the bisector plane and is inclined to the trigonal plane at an angle 6°23'+1', $P_{10}=8.405\cdot10^{-21}$, $P_{20}=0.564\cdot10^{-21}$, $P_{30}=0.743\cdot10^{-21}$ g-cm/sec. The mean squared error in the determination of the cross section when the Fermi surface is approximated by an ellipsoid is 1.26%, much larger than the measurement error ~0.2–0.3%.

An analytic expression describing the shape of the electron Fermi surface with accuracy 0.2–1% was obtained in[37] by approximating the values of $S(\vartheta,\varphi)$ by a spherical-harmonics series, as proposed by Muller.[38] As a result, it was possible to calculate the principal geometrical characteristics of the Fermi surface, particularly the values of the momenta along the principal axes (see Table III) and the principal curvature radii, whose values were $0.0518\cdot10^{-21}$ (in the C_1, C_2 plane) and $0.0558\cdot10^{-21}$ g-cm/sec in the direction of the 1 axis, 177×10^{-21} and $0.983\cdot10^{-21}$ g-cm/sec in the direction of the 2 axis, and $163\cdot10^{-21}$ and $0.422\cdot10^{-21}$ g-cm/sec in the direction of the 3 axis. The value of $\partial^2S/\partial P_z^2$ in the direction of the 1 axis is 0.0243 ± 0.0003, which is less by a factor 1.72 than the value obtained for the ellipsoid with the dimensions given in Table III.

The value obtained in[37] for the volume of the electron surface was $V_e=(14.66\pm0.01)\cdot10^{-63}$ g³cm³/sec³.

The combined volume of the three electron surfaces is $3V_e=(43.98\pm0.04)\cdot10^{-63}$ g³cm³/sec³ and the electron

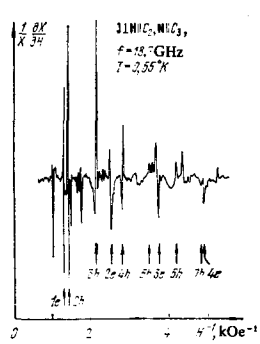

FIG. 8. Typical plot of the cyclotron resonance for a microwave current $\mathbf{J}\perp\mathbf{H}\parallel C_2$, $\mathbf{N}\parallel C_3$, $f=18.7$ GHz, $T=0.65$ K. The peaks $1e$, $2e$, ..., $2h$, ... are the cyclotron resonances for heavy electrons and holes with $n=1,2,\ldots$, respectively. Other singularities are connected with the turning points in the spectrum of the magnetoplasma waves (~1 kOe), for the cyclotron waves (structure between $2h$ and $3h$, $3h$ and $2e$, and $4h$ and $5h$), and the waves produced as a result of the anisotropy of the Fermi surface (near $3e$ and $6h$).

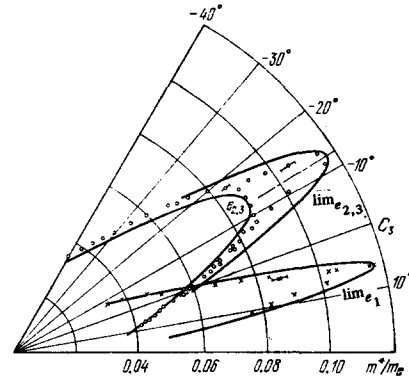

FIG. 9. Anisotropy of the effective masses of the electrons in the binary plane on central orbits ($e_{2,3}$) and at the limiting points ($\lim_{e_1}$, $\lim_{e_{2,3}}$). Solid lines—ellipses with axes equal to the maximum and minimum values of the corresponding masses.[41]

concentration is 3.015×10^{17} cm^{-3}. Using the hole sections given in Table III and assuming the hole Fermi surface to be an ellipsoid, we obtain $V_h=(43.99\pm0.05)\cdot10^{-63}$ g³cm³/sec³, which coincides with $3V_e$.

There are known direct methods for determining the dimensions of the Fermi surface, based on the study of the radio-frequency size effect[39] and of the geometrical ultrasound-damping oscillations.[40] The results obtained in these studies agree within the limits of the measurement errors, ~1–2%, with those described in the second section.

b) Measurement of the effective masses by the cyclotron-resonance method

The most detailed investigations of cyclotron resonance at $\mathbf{H}\perp\mathbf{N}$ ($\mathbf{N}$ is the normal to the flat surface of the sample) in bismuth were carried out in[41,42], and agree completely with one another within the limits of the measurement errors ~1–6%. The results of[41] were subsequently improved by us (see Table III) by carrying out measurements on samples of higher quality, with a residual relaxation time that reached ~2 nsec for the electrons and ~5 nsec for the holes.[43] The narrowing of the resonance lines not only increased the accuracy with which their position was measured, but also made it possible to interpret the complicated picture of the field dependence of the impedance, due both to the superposition of resonances from different sections of the Fermi surface and to the appearance of signularities connected with the end points of the spectra of the magnetoplasma, cyclotron, and other waves (Fig. 8).[44–47]

Figures 9 and 10 show the anisotropy of the electron masses in the binary planes and of the electrons and holes in a plane perpendicular to the 1 axis of one of the electron surfaces, as measured in[41]. It was established from the x ray diffraction pattern of this sample that the electron Fermi surface is oriented relative to the directions in the Brillouin zone in the manner shown in Fig. 4, i.e., the angle of inclination is positive in accordance with the notation of Falicov and Lin.[48] The

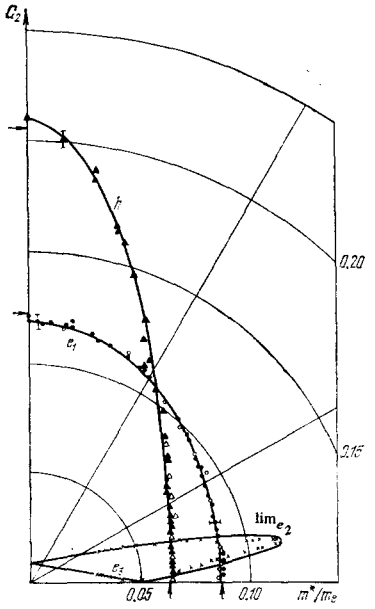

FIG. 10. Anisotropy of the effective masses in a plane perpendicular to the 1 axis of one of the sections of the Fermi surface corresponding to a mass e_1. e_3—electrons on the central orbit, $\lim_{e_3}$—at the limiting point, h—holes.[41] The arrows mark the mass values measured in[42].

same sign was obtained for the inclination angle by Brown *et al.*[49]

An interesting result of the investigation of the cyclotron resonance was the observation of a difference between the masses on the central sections and at the limiting points (Figs. 9 and 10; see Table III). This provides direct experimental proof that the electron Fermi surface is not an ellipsoid: it is known that in the latter case the effective mass is independent of P_z.

In general outline, the anisotropy of the cyclotron masses corresponds to the model whose scheme is shown in Fig. 4. It is possible to trace on the angle diagram (see Fig. 9) the deviations from the ellipsoidal model for the electrons—the change of the mass of the central section near the extremal value is smaller than for an ellipsoid and the change for the mass at the limiting point is faster.

Cyclotron resonance in bismuth in a Faraday geometry, i.e., at $\mathbf{H} \parallel \mathbf{N}$, was investigated by Galt *et al.*[5] In measurements of the absorption of circularly polarized waves, they found the carrier current to be positive. Subsequently, an investigation of the transverse focusing of the electrons[50] and the numerous studies of the change of the shape of the Fermi surface of bismuth doped with a donor or acceptor impurity, has confirmed the results of[5] (see, e.g., the article by Brandt, Yastrebova, and Ponomareva[51] and the earlier references cited therein).

c) Magnetoplasma waves. Electron density

Since bismuth is a compensated metal with ${}^eN = {}^hN$ it follows that waves analogous to the Alfvén waves and the fast magnetosonic wave of magnetohydrodynamics can propagate in it in strong fields. The wave dispersion law at $\Omega/\omega \gg 1$ and for a quadratic isotropic spectrum takes the form (see, e.g., [46])

$$\varkappa_1^2 = \frac{4\pi\omega^2}{H^2} N ({}^em + {}^hm),$$
$$k_2^2 = \frac{4\pi\omega^2}{H^2 \cos^2\vartheta} N ({}^em + {}^hm); \qquad (6')$$

ϑ is the angle between $\mathbf{k}$ and $\mathbf{H}$. At an arbitrary carrier spectrum, relations (6) retain the same form when $N({}^em + {}^hm)$ are replaced by the components of the mass-density tensor $NF_{ik}^j(m)$ (j designates the direction of $\mathbf{H}$), which can be calculated in the quasiclassical limits from the formulas obtained by Fal'kovskiĭ.[52] The calculations are particularly simple for an ellipsoidal Fermi surface. This approximation turns out to be sufficient for bismuth, inasmuch as in a large number of cases of practical importance the overwhelming contribution to the mass density is made by the holes. For example, at $\mathbf{H} \parallel C_1$ and $\mathbf{k} \parallel C_3$ the contributions of the holes, whose surface is ellipsoid, is 98.5% accurate to ~0.1%.

The wave velocities were measured in[53] for all rational directions of $\mathbf{H}$ and $\mathbf{k}$ agreed within $\lesssim 10\%$ with those calculated for a Fermi-surface model consisting of one hole and three electron ellipsoids. More accurate later measurements and calculations of $NF_{ik}^j(m)$, using more precise spectrum parameters, decreased the difference to $\lesssim 1\%$[54] (Table IV).

Thus, the Fermi surface of pure bismuth consists of three electron ellipsoids and one hole ellipsoid, and there are no other carrier groups. Taking into account the lattice symmetry (D_{3d}), we find that the extrema of the conduction bands can be located only at the Brillouin-zone points L or X, and those of the valence band at T or Γ. Koenig *et al.*,[55] analyzing the results of experiments in which the electron-hole recombination times were obtained, have found an additional restriction on the possible location of the carriers in the Brillouin zone, namely, they should be either at the points L or T, or at X and Γ. A choice between these two cases can be made at the present time only by using a theory that demonstrates that the first of them is realized, namely, the electrons are localized at L and the holes at T (see Sec. a of Ch. 2).

d) Measurements of electron velocity. Magnetic surface levels

Knowledge of the shape of the Fermi surface and of the effective masses on this surface makes it possible

TABLE IV. Components of the mass-density tensor.[54]

	NF_{22}^1	NF_{33}^1	NF_{11}^2	NF_{11}^3
	m_e, 10^{-17} см$^{-3}$			
Experiment	2.09±0,01 *)	0.248±0,001	1,009±0,005	2.19±0,01
Calculation	2,115±0,02	0.248±0,002	1,00±0,01	2,17±0,02

The superscript labeling the NF components indicates the direction of the magnetic field.

*Measured for a sample with the angle between N and C_3 equal to 3°.[5] The calculation was made for this orientation.

in principle to calculate the carrier velocities. This problem, however, can be solved simply only for simple orbits. For example, for holes, taking into account the axial symmetry of the Fermi surface, we obtain for the central orbit at $\mathbf{H} \parallel C_3$

$$v_\perp = \frac{1}{m_3^*}\sqrt{\frac{S_3}{\pi}} = (2.52 \pm 0.015)\cdot 10^7 \text{ cm/sec}.$$

Direct methods for the measurement of the Fermi velocity are available. These include observation of the Doppler-shifted cyclotron resonance and investigations of the Landau damping of magnetoplasma waves.[56] The experiments carried out in[56] have made it possible to measure the velocities of the electrons and holes accurate to ~5–10%. Naturally, within the limits of this error the velocities coincided with those expected for the ellipsoidal model.

The electron velocities can be measured with high accuracy by studying resonance transitions between magnetic surface levels.[7] The magnetic surface levels are the results of quantization of the periodic motion of the electrons that experience multiple specular reflections from the sample surface. The energy levels of these electrons are given by[7]

$$E_n = \zeta_n \left(\frac{e^2\hbar^2}{2Pc^2}\right)^{1/3} v_F H^{2/3}, \qquad (7)$$

where ζ_n is the n-th root of the Airy function,

$$\zeta_n \approx \left[\frac{3\pi}{2}\left(n - \frac{1}{4}\right)\right]^{2/3};$$

P is the curvature radius of the trajectory in phase space; v_F is the velocity in the direction perpendicular to the field.

When the magnetic field changes, resonances are observed at an external-field frequency

$$\omega = \omega_{nm} \equiv \frac{E_n - E_m}{\hbar}. \qquad (8)$$

The energy E_n (formula (7)) depends only on $v_F/P^{1/3}$. Since the curvature radii can be calculated from the known model of the Fermi surface (see Sec. a of Ch. 3), observation of the resonance transitions makes it possible to determine v_F. The electron velocity measured by us along the binary axis is $v_2 = (10.0 \pm 0.1)\cdot 10^7$ cm/sec.[12] Koch and Jensen[58] have found that the electron velocity on the minimal section of the Fermi surface varies in accordance with an elliptic law and amount to $v_2 = (9.9 \pm 0.1)\cdot 10^7$ and $v_3 = (7.5 \pm 0.1)\cdot 10^7$ cm/sec. We have modified here their values by adding a correction ~3% due to the line shape,[59] and by introducing more accurate curvature radii.[37]

Takaoka *et al.*[60] observed, in the measurement of the anisotropy of the magnetic surface levels in the binary plane, deviations from the ellipsoidal model, qualitatively similar to those observed in the investigation of the quantum oscillations of the conductivity (see Sec. a of Ch. 3) and of the cyclotron resonance (Sec. b of Ch. 3). Calculations by their results yields $v_1 = 8.9\times 10^6$ cm/sec.

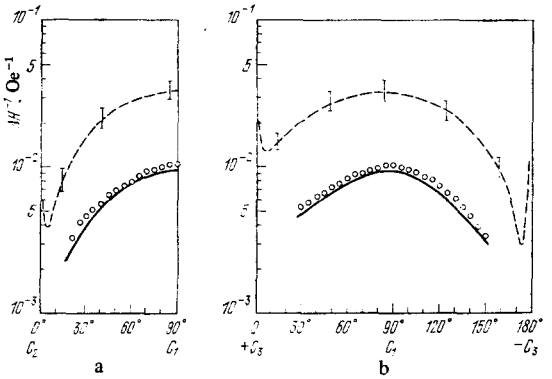

FIG. 11. Period of the magnetoacoustic oscillations on the electron surface vs. the direction of the field H.[61] The wave vector k is parallel to C_1. Circles—experiment, dashed line—calculation by the ellipsoidal model, solid line—calculation by the model of[37], which is based on inversion of the data on the Shubnikov—de Haas effect.

e) Magnetoacoustic resonance

When ultrasound is considered at an angle to the magnetic field, the electrons for which the condition

$$|\omega - \overline{\mathbf{kv}}| = n\Omega, \qquad (9)$$

is satisfied absorb resonantly the wave energy if the orbit has points for which $\mathbf{k}\cdot\mathbf{v} = 0$. The latter conditions that the trajectory has sections parallel to the wave front and when the electrons move along these trajectories they interact effectively with the waves. When the magnetic field is decreased from a sufficiently large value, periodic oscillations of sound absorption are observed and are caused by the fact that the resonant electrons with $n = 1, 2, 3, \ldots$ become effective. According to Golik *et al.*[61] the period of these oscillations is exceedingly sensitive to the shape of the Fermi surface. Figure 11 shows the values of the periods of the magnetoacoustic resonance of the electrons measured in[61], compared with those calculated by the ellipsoidal model and by the numerical model (see Sec. a of Ch. 3). It is seen that the small deviations from ellipsoidal leads in this case to a change of the period by several times.

Measurements of the magnetoacoustic resonance for holes have shown that their Fermi surface differs from an ellipsoid by not more than ~0.1%.[61]

f) Cyclotron resonance on non-extremal orbit[62]

Cyclotron resonance is observed as a resonant singularity of the surface resistance of the sample as a function of the magnetic field. In the case of a convex Fermi surface and a non-quadratic spectrum, these singularities occur at the end of the smooth spectrum of the cyclotron frequencies $\Omega = \Omega(P_z)$, corresponding to the central section at the limiting point. The truncation of the trajectories whose diameters are larger than the thickness D of the plane-parallel sample produces an aritificial end point Ω_{ep} of the spectrum of the electrons moving on closed trajectories without colliding with the sample surface. The cyclotron resonance is observed at this artificial end point of the spectrum. The condi-

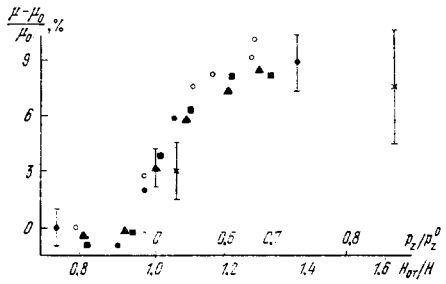

FIG. 12. Dependence of the effective mass of the electrons at $H \parallel C_2$ on the value of H_{∞}/H.[62]

tion for its realization is the simultaneous satisfaction, for a certain intermediate section of the Fermi surface, of the following equations (the x axis is parallel to the sample surface):

$$2P_x(P_z) = \frac{e}{c} HD, \qquad \frac{\omega}{n} = \Omega_{cp} = \frac{eH}{m^*(P_z)c}. \tag{10}$$

Decreasing the field shifts the boundary section of the complex Fermi surface away from its central section to the limiting point, and at $n \gg 1$ the conditions (10) are satisfied on many intermediate sections. It thus becomes possible to measure $m^*(P_x)$. Figure 12 shows the dependence, measured in[62] of the effective mass of the electrons of the small section at $\mathbf{H} \parallel C_3$. No one has yet succeeded in observing cyclotron resonance on non-extremal sections for other groups.

The experiment described above provides detailed information on the spectrum of bismuth at the Fermi level. It is most important that all the results are in good agreement.[12,37] Their compatibility is manifest, in particular, in the fact that it is possible to describe the entire aggregate of the data by a relatively simple dispersion equation (the coordinate axes correspond to Fig. 4)[35]

$$E_+ \times E_- = E_g \times \sum_1^3 \frac{P_i^2}{2m_i} - \left(\frac{P_3^2}{m_{13}^2} + \frac{P_3^2}{m_{12}^2}\right) P_1^2, \qquad E_\pm = E \mp \frac{1}{2}\left(E_g + \frac{P_1^2}{m_{11\pm}} + \frac{2P_1P_3}{m_{13\pm}}\right), \tag{11}$$

This, as can be readily seen, differs from Cohen's spectrum (3) in the presence of the following terms: $2P_1P_3/m_{13\pm}$, which describes the asymmetry of the surface, $E_gP_1^2/2m_1$, which leads to a deviation of the $E(P_1)$ plot from a parabola and brings the spectrum closer to the Lax model, and the fourth-order terms $\sim P_i^2P_1^2$.

The spectrum (11) describes, accurate to ~0.5% (which is close to the measurement accuracy), the results of the experiments considered in Secs. a–d of Ch. 3, if the coefficients are equal to: $E = 35.6$ meV, $E_g = 13.5$ meV, $m_{11-} = 1.32$, $m_{11+} = 1.46$, $m_{13-} = 0$, $m_{13-} = 7.9$, $m_1 = 0.345$, $m_2 = 1.196 \cdot 10^{-3}$, $m_3 = 2.08 \cdot 10^{-3}$, $m_{12} = 0.28$, $m_{13} = 0.24$. All the masses are in units of m_e. The angle of inclination of the 1 axis to the trigonal plane is 6°23′.

The agreement between the results of the measurement of the magnetoacoustic resonance (see Sec. e of Ch. 3) and of the cyclotron resonance on the nonextremal orbits (Sec. f of Ch. 3), on the one hand, and the spectrum (11) on the other, has not been verified.

At present it is difficult to say to what extent the spectrum of McClure and Choi[35] describes the electrons at energies that differ noticeably from the Fermi energy, since the corresponding energy levels in a magnetic field were not calculated. This makes difficult a comparison with experiment on magnetoreflection (see Sec. b of Ch. 4) and the measurement of conductivity in a quantizing field (Ch. 5). At any rate, it provides a good interpolation model of the electron Fermi surface, one that is more convenient than the expansion in spherical harmonics proposed in[37].

No deviation from ellipsoidal shape was observed for the hole Fermi surface. According to magnetoacousto-optical investigations (Sec. e of Ch. 3), the possible deviations are $\lesssim 0.1\%$. The total volume occupied by the surface in momentum space, assuming that the surface is ellipsoidal, is equal, within 0.1%, to the combined volume of the three electron surfaces.

Using the hole cross section and masses listed in Table III, we get

$$\frac{S_1/m_1^*}{S_3/m_3^*} = 1.003 \pm 0.005.$$

It is known that for an ellipsoid this ratio should be equal to unity. Thus, to determine the possible nonparabolicity of the hole spectrum from measurements on the Fermi level, the measurement accuracy must be increased by one more order of magnitude.

4. INVESTIGATIONS IN THE INFRARED BAND

a) Spectral measurements without a magnetic field

Investigations of bismuth in the range ~10–100 μm have revealed a plasma resonance and an interband absorption edge.[63] An absorption edge connected with direct interband transitions at the point L was observed[63] at $\lambda \approx 17$ μm. The photon end-point energy $E_{ph} \approx 68$–70 meV attests to the presence of an anomalously small (~10–20 meV) energy gap in the electron spectrum. Thus, this experiment served as the basis for the two-band model.

It is known that the behavior of a metal at frequencies close to the plasma frequency is determined by the lattice dielectric tensor ε_{jk} and by the high-frequency conductivity tensor σ_{jk}. Recognizing that the electrons on the Fermi level take part in the production of the screening currents, σ_{jk} can be calculated, accurate to several percent, by using the formulas obtained by Lax *et al.*[64] for the ellipsoidal model. Substituting in these formulas the parameters of the ellipsoid (Ch. 3), we obtain

$$\sigma_{jk} = \frac{iNe^2}{\omega}\left\{\begin{matrix}\frac{1}{2^6 m_2} + \frac{1}{\hbar m_2} & (j=k=1,2)\\ \frac{1}{e m_3} + \frac{1}{\hbar m_3} & (j=k=3)\end{matrix}\right\} = \frac{iNe^2}{m_e\omega}\left\{\begin{matrix}96.2,\\ 98.5.\end{matrix}\right. \tag{12}$$

Maxwell's equations with allowance for the Debye cur-

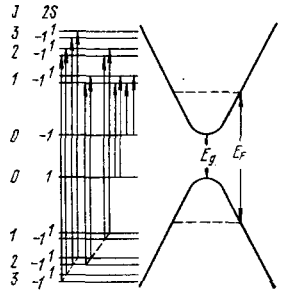

FIG. 13. Scheme of resonant transitions observed in experiment on magnetoreflection.[21]

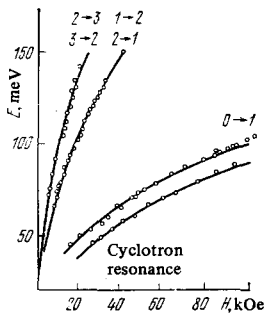

FIG. 14. Plot, for light electrons, of the energy of the interband transitions and of the cyclotron resonance against the field $\mathbf{H} \parallel C_1$. Circles—experiment. Lines—calculation by the two-band model.[67]

rents in the expression (12) for the conductivity yields for the wave number the expression

$$k^2 = \frac{\omega^2}{c^2}\left(\varepsilon_{jj} - \frac{4\pi N e^2 f_{jj}(m)}{m_e \omega^2}\right). \tag{13}$$

The relation (13) was experimentally verified by Boyle and Brailsford,[63] who investigated the interference of waves passing through a thin sample. On the basis of this experiment it was found that $\varepsilon_{11} = \varepsilon_{22} = \varepsilon_\perp = 100$. Kulakovskiĭ and Egorov[65] obtained $\varepsilon_\perp = 110 \pm 10$ from the light-reflection coefficient. For the plasma-resonance frequency corresponding to $k = 0$, at a polarization perpendicular to C_3, values 158 ± 3 cm^{-1} (2.98×10^{13} sec^{-1})[63] and 2.98×10^{-13} sec^{-1} [65] were obtained. Substituting in (13) the numerical value of σ_{11} from (12), we get $\varepsilon_\perp = 104$. For light polarized along the trigonal axis, the plasma-resonance frequency is 187 cm^{-1},[63] thus yielding $\varepsilon_{33} = \varepsilon_\parallel = 76$.

Experiments performed in a wider range of photon energies have revealed the appearance of succeeding spectral singularities only starting with an energy 0.69 eV[18] (see Table II).

b) Magneto-optical investigations

Absorption resonances connected with interband and intraband resonant transitions at the point L between the Landau levels in a magnetic field were investigated in[21,66–68]. According to[21,69] the allowed transitions are those with $\Delta j = 1$ where $j = n + (1/2) + s$, and are shown schematically in Fig. 13. The dependence of the energy of these transitions on the magnetic field, obtained in[67], is shown in Fig. 14 at $\mathbf{H} \parallel C_1$.

From the two-band-model spectrum (2), taking into account the inequality $jeH\hbar/m_0^* c \gg E_g/4$, which is satisfied under the experimental conditions, we obtain for the transition frequency at $j \neq 0$, accurate to $\lesssim 1\%$

$$\hbar\omega_{j,j+1} = \sqrt{E_g \frac{e\hbar H}{m_0^* c}}\left(\sqrt{j} + \sqrt{j+1}\right). \tag{14}$$

The presence of other bands lifts the degeneracy of the j-th level (at $j \neq 0$), a fact that manifests itself, for example, in the spin splitting of the quantum oscillations (see Sec. a of Ch. 3). However, for interband transitions with $\Delta s = 0$, the spin splitting linear in the field has a value $\sim (\Delta_+ + \Delta_-)/8m_0^* j \lesssim 1\%$,[34] which is less than the line width of the resonant transition. The possible effective-mass renormalization due to the remote band can lift the degeneracy of the frequencies of the transitions $j \to j+1$ and $j+1 \to j$. Inasmuch as no line splitting was observed in experiment, Maltz and Dresselhaus[67] have proposed that there is no mass renormalization and that[4] $\Delta_+ = \Delta_-$. Estimates show that the effects quadratic in the field and due to the influence of the remote bands are small even at the maximal fields $H \approx 100$ kOe at which the experiments were performed. Thus, the use of the two-band model to describe interband transitions with $j \neq 0$ is perfectly justified. Relation (14) agrees well with experiment (Fig. 14) at $E_g e\hbar/m_{01}^* c = 93.5 \pm 1$ meV^2/kOe.[67,68]

In contrast to the transitions with $j \neq 0$, the transition frequencies at $j = 0$ depend substantially on E_g. Vecchi *et al.*[21] have shown that all four possible transitions, with and without change of spin, shown in Fig. 13 are allowed. Their frequencies are determined by formula (5) with $\Delta_+ = -\Delta_- = -(8.7 \pm 1) m_e^{-1}$, corresponding to a decrease of the gap between the bands in weak fields at a rate of 0.09 meV/kOe and to $b = 1.5$. The value obtained earlier by Vecchi and Dresselhaus for the last parameter was ~ 3.5.[68] The new value, however, seems more justified, inasmuch as the measurements in[21] were made in a larger range of magnetic fields, and the parameters were determined by comparing the experiments with the calculated dependence of the reflection coefficient on the field. We shall return to the results obtained here in Ch. 6.

Magneto-optical investigations are of particular interest in that raising the sample temperature all the way to ~ 300 K does not influence very strongly the resolving power of the method. The reason is that even at $T = 0$ K the Landau levels are greatly broadened by the electron-electron interaction of excitations whose energy greatly differs from the Fermi energy. Therefore the characteristic temperatures at which further broadening of the levels set in are $\sim T_F \approx 100$ °K. Vecchi and Dresselhaus[70] succeeded in measuring the temperature dependence of $E_g(T)$ and $(e\hbar/m_0^* c) E_g(T)$, which are described by the formulas (at $\mathbf{H}$ parallel to the 1 axis)

$$E_g(T) = 13{,}6 + 2{,}1 \cdot 10^{-3}\, T + 2{,}5 \cdot 10^{-4} T^2 \text{ (meV)},$$
$$E_g \frac{e\hbar}{m_{01}^* c} = 94{,}1 - 8{,}5 \cdot 10^{-2} T - 2{,}4 \cdot 10^{-4} \text{ (meV}^2\text{/kOe)}.$$

[4] Since the lines have a width on the order of several percent, appreciable deviations from these results are admissible.[12] The exact values, however, cannot be indicated at the present time.

In this section we have dealt so far with the spectrum parameters of H parallel to the 1 axis. As expected, at other magnetic-field directions, making an angle ϑ with the 1 axis ($\vartheta \lesssim 70-80°$), to describe the experimental results it suffices to replace m_{01}^* by $m_{01}^*/\cos\vartheta$ and to assume that the relative spin splitting is unchanged. So far, no magneto-optical resonances connected with interband transitions have been observed for heavy electrons at $\mathbf{H} \parallel C_2$ and $\mathbf{H}$ parallel to the 3 axis for holes.

5. INVESTIGATION OF BISMUTH IN THE QUANTUM LIMIT

a) Principle of method

Pure bismuth can be used to investigate carriers at various energies because of the change of the end-point energy in a strong magnetic field. For example, in a field $H > 26$ kOe directed along the bisector axis C_1, each of the electron conduction bands below the Fermi level is left with only one Landau level. The electron density at these levels at $T = 0$ K is[36]

$$N = \frac{2eHP_z}{(2\pi\hbar)^2 c} \tag{15}$$

(P_z is the maximum electron momentum in the field direction), so that when the field is increased the number of electrons and holes is kept equal by a shift of the Fermi energy E_F, which leads to a decrease of P_z.

A favorable circumstance that facilitates the study of bismuth in a quantizing field is the strong anisotropy of the Fermi-surface sections. Therefore, when the quantum-limit conditions have already been realized for the electrons, the holes still remain in the quasiclassical magnetic-field region, and it is possible to observe the magnetic-moment or conductivity oscillations due to quantization of the hole spectrum.[17,21,54,71]

Another possibility is to measure the velocity of the magnetoplasma waves and to determine in this manner the variation of the mass density with changing fields,[54,72,73] or else to determine the effective mass directly by measuring the cyclotron resonance.[20]

It was shown in[74] that a single experiment in which both effects are investigated yields direct information on the changes of the Fermi energy and of the carrier density. We shall consider the capabilities of such a method qualitatively within the framework of the quasiclassical approach. For holes at $\mathbf{H} \parallel C_1$ it is perfectly satisfactory up to the fields ~100 kOe to which a quantum number $n \geq 4$ corresponds. In the classical case, the field corresponding to the n-th oscillations is connected with the cross section by the known relation (at $g = 0$)

$$S(H_n) = \left(n + \frac{1}{2}\right)\frac{eh}{c}H_n. \tag{16}$$

From (16) we obtain for the carrier density

$$\frac{N(H)}{N(0)} = \left[\frac{S(H)}{S(0)}\right]^{3/2}. \tag{17}$$

The velocity of the magnetoplasma (Alfvén) waves, for carriers with an anisotropic spectrum (see Sec. c of Ch. 3), is

$$vH^{-1} = [4\pi N\,(^hm + {}^em)]^{-1/2} \approx [4\pi N\,(H)^h m\,(H)]^{-1/2}. \tag{18}$$

Comparing (17) and (18) we see that simultaneous measurement of these quantities yields the functions $N(H)$ and $m(H)$. Recalling the definition $m = (1/2\pi)\partial S/\partial E$ and determining from (17) and (18) the function $m(S)$, we obtain

$$E_F(H) - E_F(0) = \int_{S(0)}^{S(H)} \frac{dS}{2\pi m\,(S)}. \tag{19}$$

Thus, the experiment yields such quantities as $N(H)$, $E_F(H)$, $m(E)$, and $S(E)$. By using a suitable model of the spectrum, for example the two-band model (1), it is easy to determine from $m(E)$ and $S(E)$ the size of the gap and $E_F(0)$. By the same token, it is possible to obtain in principle a complete description of the carrier spectrum.

b) Measurement of $N(H)$ and $E_F(H)$

Let us examine in greater detail the results of[21,54,71]. Compared with the earlier investigations in this field,[17,72,73] the measurements of[54] were made on samples of better quality, characterized by a residual-relaxation time ~2–5 nsec, and at a lower temperature, $T \approx 0.4$ K. As a result, the resolution and the accuracy of the measurements of the quantum oscillations of the conductivity (Fig. 15) and of the velocity of the magnetoplasma waves were higher by one order of magnitude. This has made it possible, in particular, to detect the errors of the preceding studies (see[12]). The measurements in[21,71] were performed in substantially stronger fields than in[54].

The values of the wave number k in strong fields, when the displacement currents must be taken into account because of the drop of the conduction currents, are con-

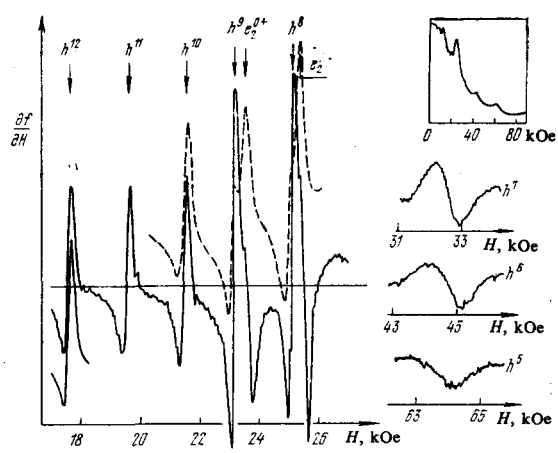

FIG. 15. Quantum oscillations of the resistance at 10 MHz, $T = 0.4$ K, and $\mathbf{H} \parallel C_1$.[54] The arrows show the positions of the oscillations of order n for the holes (h) and electrons (e). The insert shows a plot of the quantum oscillations of the conductivity from[17].

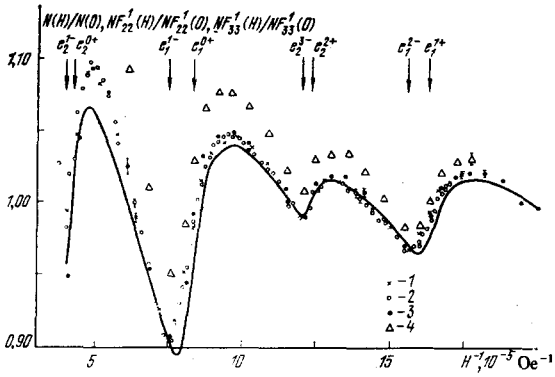

FIG. 16. Dependence of the hole density (1) and of the mass densities NF_{22}^1 (2) and NF_{33}^1 (3) on a field H parallel to C_1. 4—value of $NF_{33}^1(H)$ assuming $\varepsilon = 0$. The wave frequency is 27.87 GHz. The arrows mark the positions of the quantum oscillations of order n for electrons with one axis parallel to H(e_2) and with the 1 axis making an angle 60° with H. The plus and minus signs correspond to the different spin projections.[54]

nected with the mass-tensor components by the dispersion equation (at $\mathbf{H} \parallel C_1$ or $\mathbf{H} \parallel C_3$ and $\mathbf{k} \perp \mathbf{H}$)

$$k^2 - \varepsilon_{\alpha\alpha}\frac{\omega^2}{c^2} - i\,\frac{4\pi\omega^2 c}{H^2}\,NF^j_{\alpha\alpha}(m) = 0. \qquad (20)$$

The indices α and j indicate the wave polarization direction perpendicular to H and k and the direction of the field H, respectively. $\varepsilon_{\alpha\alpha}$ are the components of the dielectric tensor of the lattice.

The contribution of the electrons to $NF_{22}^1(m)$ and $NF_{33}^1(m)$ is relatively small (~1.5 and 22.5%, respectively) and can be taken into account by calculation. Figures 16 and 17 show the plots of $N(H)$ and of the contribution of the holes to $NF(H)$ obtained in[54] at $\mathbf{H} \parallel C_1$.

An analysis of the plots shown in Fig. 16 and of the analogous ones at $\mathbf{H} \parallel C_3$ has shown that in strong fields the high-frequency conductivity receives an appreciable contribution from the displacement current. The components $\varepsilon_{33} = 65 \pm 5$ and $\varepsilon_{11} = \varepsilon_{22} = 100 \pm 10$ were determined by choosing the lattice dielectric constant ε such that

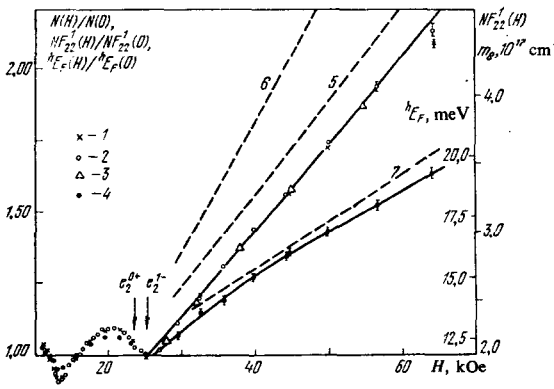

FIG. 17. 1, 2—the same as in Fig. 16. 3—$NF_{22}^1(H)$ at $f = 17.6$ GHz. 4—Fermi energy of holes. The dashed lines 5 and 6 show the values of $NF_{22}^1(H)/NF_{22}^1(0)$ obtained in[72,73], 7—$E_F(H)/E_F(0)$ from[17]. The right-hand scale pertains only to the solid lines.

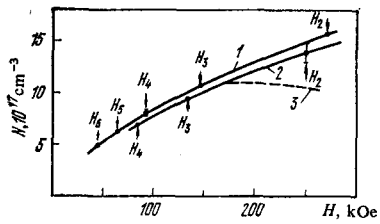

FIG. 18. Plots of $N(H)$ at $\mathbf{H} \parallel C_1$ (1) and $\mathbf{H} \parallel C_2$ (2), calculated from the positions of the quantum oscillations of the holes (marked by arrows) assuming an ellipsoidal model. The value of H_2 is taken from[71], H_3 and H_4 are from[21], and the remainder from[54]; 3—calculation of $N(H)$ using the electron-spectrum model obtained in[21] at $\mathbf{H} \parallel C_2$.

the functions $N(H)$ and $NF(H)$ coincide in the field regions $H \lesssim 25$–30 kOe. These values are in good agreement with those given in the fourth paragraph of Sec. a of Ch. 4.

A comparison of $N(H)$ and $NF_{22}^{(1)}(H)$ at $H = 65$ kOe (see Fig. 17) shows that the effective mass of the holes is practically independent of the field. This means that the hole spectrum is quite close to quadratic. Possible deviations from a quadratic spectrum can be estimated by assuming a two-band-model spectrum with $^hE/^hE_{g\,eff} \ll 1$. From the ratio

$$\frac{NF(H)/NF(0)}{N(H)/N(0)} = \frac{^hm_1^*(H)}{^hm_1^*(0)} = 1.017 \pm 0.01$$

we obtain $^hE_{g\,eff} = 0.9^{+0.9}_{-0.4}$ eV. Knowing the section of the Fermi surface and the hole mass, we calculate the mass at the top of the valence band, $^hm_{01}^* = 0.206 \pm 0.003\, m_e$ and the hole Fermi energy $^hE_F = 11.72 \pm 0.10$ meV reckoned from the top of the band. The plot of $^hE_F(H)$ based on the results of experiments using the two-band-model spectrum is shown in Fig. 17. By using the same model, it is possible to determine $N(H)$ and $E_F(H)$ from the results of[21,71] for fields up to ≈300 kOe. A plot of $N(H)$ is shown in Fig. 18. Measurements[54] performed at $\mathbf{H} \parallel C_3$ yielded a hole g-factor $g_3 = 4.26 \pm 0.02$.

6. SPECTRUM OF THE ELECTRONS OF THE LOWER LANDAU LEVEL

One of the main problems encountered in the investigation of bismuth is the determination of the parameters of the electron spectrum at the bottom of the conduction band. The difficulty in solving this problem is due to the fact that in pure bismuth $E_F = E_{ph}/2 = 35$ meV and exceeds greatly the value 13.6 meV obtained for E_g from magneto-optical measurements. As a result, the parameters of the spectrum at the Fermi level depends little on E_g. Thus, for example, it is easy to obtain from the two-band-model spectrum (1) the ratio

$$\frac{S_1}{m_1^*} = \frac{\pi}{2}E_{ph}\left(1 - \frac{E_g^2}{E_{ph}^2}\right). \qquad (21)$$

Substituting here the corresponding numerical values, we find that the factor in the parentheses differs from 1 by less than ~4%. On the other hand, we have $2S_1/\pi m_1^* E_{ph} = 1 \pm 0.02$. This example shows therefore that, on the one hand, the spectrum in a direction perpendic-

ular to the 1 axis is in fact quite close to the two-band spectrum. On the other hand, it is clear that from measurements at the Fermi level it is practically impossible to determine the parameters of the spectrum at the bottom of the band, all the more since one can expect from the very outset the deviations from the simple models to be of the same order of magnitude as the difference between the spin and orbital splittings, i.e., ~10%. Such differences were in fact observed in experiment (see Ch. 3). To establish the spectrum at the bottom of the conduction band, it is obviously necessary to investigate effects in which electrons located at the bottom of the band take part. Such a possibility is afforded by performing measurements in strong magnetic fields, when only one Landau level remains below the Fermi level. By the same token, the problem reduces to a determination of the spectrum of the lower Landau level.

One experiment of this kind—measurements of the frequencies of the intraband and interband transitions—was described in Sec. b of Ch. 4. There is one other possibility of investigating the electrons of the lower Landau level, and is connected with the appreciable displacement of the Fermi level and its approach to the bottom of the band when a strong magnetic field is superimposed. Since the observation of the holes makes it possible in this case to determine the change of the Fermi energy and of the electron momentum in the field direction (see Sec. b of Ch. 5), it becomes possible to establish the curvature of the conduction band and its shift under the influence of the field.

The determination of the connection between the shift of the Fermi level and the characteristics of the electrons is made complicated by the fact that at those field directions at which this influence is strongest, for example at $\mathbf{H} \parallel C_1$, there exist non-equivalent groups of electrons. It is therefore necessary to resort to spectrum models and to attempt to determine their parameters by comparison with experiment. Such an approach was used in[12,54], in which the Fal'kovskiĭ-Beneslavskiĭ spectrum (4) was assumed for the lower Landau level. As noted in Sec. a of Ch. 2, this spectrum is valid when H is close in direction to the 1 axis.

The direction of H can be assumed to be close to the 1 axis if the effective mass m^* of the central section is close at this direction to the value

$$m^* = \frac{m_1^*}{\cos(\widehat{\mathbf{H}, \text{axis 1}})}, \qquad (22)$$

where m_1^* is the mass at H parallel to the 1 axis. It is easy to verify that the condition (22) is satisfied for the electron with an error less than ~1% if the angle between H and the 1 axis is equal to 60°. Therefore at $\mathbf{H} \parallel C_1$ the spectrum takes the form (4) for all the electron groups. For the electron sections in which the direction of the 1 axis makes an angle ~60° with the field it is then necessary to put $m_g = m_1/4$ and $a = a_1/2$, for in the case the effective mass is twice as large as at H parallel to the 1 axis, and the relative spin splitting remains unchanged.

The experiment described in the preceding section

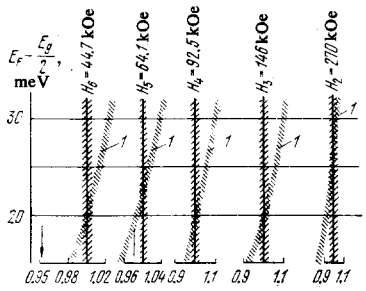

FIG. 19. Calculated values of H_n for hole quantum oscillations of order n vs. the Fermi energy of the electrons—hatched strips 1. The hatching of the vertical lines shows the measurement error. The arrows indicate the calculated values of H_n from[21].

makes it possible to determine the values of the parameters of the spectrum (4), if the following conditions are taken into account:

a) ${}^eN(H) = {}^hN(H)$ independently of the field.

b) Since the electron energy connected with the cyclotron motion in a field ~100 kOe is ~0.1 eV, the additional energy due to the application of the field is $\sim 10^{-6}$ eV/atom, i.e., the band structure remains unchanged. We can therefore put

$${}^eE_F(H) = {}^eE_F(0) - \Delta E(H), \quad {}^hE_F(H) = {}^hE_F(0) + \Delta E(H)$$

(the hole energy ${}^hE_F$ is reckoned downward from the top of the valence band at $H = 0$).

c) For holes, small deviations of the spectrum from quadratic can be described by the two-band model, which leads, with the zero spin splitting taken into account, to Landau levels

$${}^hE_n\left(1 + \frac{{}^hE_n}{{}^hE_{g\,\text{eff}}}\right) = \left(n + \frac{1}{2}\right)\hbar\Omega + \frac{P_z^2}{2m_1}. \qquad (23)$$

with the parameters obtained in Secs. b of Ch. 3 and b of Ch. 5.

Assuming that the n-th quantum oscillations of the conductivity for holes (see Fig. 15) takes place in a field H_n such that ${}^hP_z^{(n)} = 0$, and taking the conditions listed above into account, we readily calculate H_n as a function of the two parameters $({}^eE_F(0) - E_g/2)$ and a.

Figure 19 shows the results of a calculation of H_n for $n = 2, 3, 4, 5$, and 6. At each value of $({}^eE_F(0) - E_g/2)$ the value of a was chosen such as to make H_7 agree with the experimental $H_7 = 32.6 \pm 0.15$ kOe. The errors in the calculated values are due to the errors in the measurement of H_7 and, to a lesser degree, of ${}^hE_{g\,\text{eff}}$.

In accordance with the calculation (see Fig. 19), we must assume ${}^eE_F(0) - (E_g/2) = 21 \pm 1$ meV and $(e\hbar/2C)\Delta_{\perp} = -0.040 \pm 0.005$ meV/kOe. These values were obtained under the assumption that the spectrum (4) corresponds exactly to the electron spectrum. To take into account the next order of perturbation theory we can introduce the energy dependence of the mass m_1, via the substitution $m_1 \to m_1[1 + (E/E_0)]$, where E_0 is a parameter that must be determined from experiment. This expression

coincides formally with the spectrum of the two-band model if $E_0 = E_g/2$. If $E/E_0 \ll 1$, this substitution is equivalent to introducing into the spectrum a term proportional to P_z^4.

Numerical calculations have shown that agreement with experiment can be obtained at $E_0 \gtrsim 0.1$ eV. The value of ${}^eE_F(0) - (E_g/2)$ at $E_0 = 0.1$ eV increases to ~25 meV, and the rate of the shift of the bottom of the band becomes equal to -0.05 meV/kOe.

Thus, assuming the spectrum of the electrons at the lower Landau level to be close to (4), we arrive at the conclusion that ${}^eE_F(0) - (E_g/2) < 25$ meV. Recalling that the energy of the edge of the interband absorption is $E_{ph} = 2{}^eE_F(0) = 68$–$70$ meV (see Sec. a of Ch. 4), we obtain $E_g \gtrsim 18$–20 meV, which exceeds noticeably the value $E_g = 13.6$ meV measured in magneto-optical investigations (Sec. b of Ch. 4). This raises the question of whether the electron spectrum (5), used by Vecchi *et al.*[21] might not describe the strong-field measurement results just as well as the spectrum (4). We note that at $P_z \neq 0$ these spectra differ not only by the term proportional to H_2 and describing the repulsion between the bands, but also in the dependence of E on P_z. Namely, the dependence investigated in[21] is characteristic of the two-band model, namely, quadratic at $|E - E_g/2| \ll E_g/2$ and becoming linear at $|E - E_g/2| \approx E_g/2$.

The results of the calculations of[21] are shown in Figs. 18 and 19. It is seen that the values of H_n (see Fig. 19), as well as those of $N(H)$, do not agree with experiment.[5] Thus, the questions of both the electron spectrum and of the exact value of E_g remain open. The motivation for the last statement is that the interpretation of the experiment in[21] was carried out for a concrete model, and it is not excluded that the use of a different model might lead to other values of the parameters.

Consider now the possibility of determining E_g from other experiments. It is obvious that the value $E_g \approx 15$ meV obtained in[17] need not be taken into account, since conceptually this is the same experiment as in[54] but its accuracy is lower by many times. The same can also be stated concerning a large number of earlier magneto-optical studies, in which substantially larger E_g were obtained because of erroneous interpretation.

We must dwell in particular detail on the frequently cited paper by Strom *et al.*,[75] who obtained $E_g = 13 \pm 2$ meV, a value that confirms the results of[21]. However, our analysis in[12] has shown that this figure can in principle not be obtained from the result of[75]. Strom *et al.* investigated cyclotron resonance at frequencies $(0.9$–$2.5) \cdot 10^{12}$ Hz ($\hbar\omega \approx 4$–10 meV ≈ 0.1–$0.3\,E_F$). Intraband resonance transitions $j \to j+1$, $j \to j+2$, $j \to j+3, \ldots$, were observed, with the lower level having at $T = 0$ an energy $\lesssim {}^eE_F$, while the upper level an energy $\gtrsim {}^eE_F$. Putting $\delta = {}^eE_F - E_j$, we obviously have $E_{j+n} \equiv {}^eE_F + \omega - \delta$. Substituting these values in (2′), performing simple algebraic manipulations, and recognizing that the mass at the Fermi level is $m^* = m_0^* E_{ph}/E_g$, we obtain an equation for the transition frequency

$$\omega\left(1 + \frac{\hbar\omega - 2\delta}{E_{ph}}\right) = n\frac{eH}{m^*c}. \tag{24}$$

According to (24), the maximum deviation of the resonance frequency from the classical value neH/m^*c is reached at $\delta = \hbar\omega$ or at $\delta = 0$, and amounts to $\pm\hbar\omega/E_{ph} \lesssim 6$–$15\%$. If it is recognized that either $\delta/{}^eE_F < \hbar\omega/2{}^eE_F \ll 1$, or correspondingly $\hbar\omega - \delta/{}^eE_F \ll 1$, then its value can be obtained from the obvious relation

$$\delta = \frac{S}{2\pi m^*}\left(1 - \frac{H}{H_j}\right), \tag{25}$$

where S is the section of the Fermi surface and H_j is the field at which the j-th Landau level intersects the Fermi level; this field is determined by investigating the de Haas–van Alphen or the Shubnikov–de Haas effect.

Thus, the entire picture of the quantum cyclotron resonance in the two-band model is determined completely by spectrum parameters known from other experiments. Substitution of the numerical values of H_j calculated from the data of Sec. a of Ch. 3 and $m^* = 0.0094\,m_e$ (Sec. b of Ch. 3) in the formulas (24) and (25) leads to an argument between the predicted position of the cyclotron-resonance lines at $\mathbf{H} \parallel C_2$ with all the lines observed in[75], with an rms error 0.4%.

As seen from (24), the transition frequencies for multiple resonances, i.e., at $n \neq 1$, do not agree with one another. Each of these resonances splits into n lines whose amplitude ratio depends on the level population and changes with increasing T. This circumstance was used by Strom *et al.*[75] to determine ${}^eE_F$. This method, however, can be used to determine only the parameter $({}^eE_F - E_j)/kT$, which determines in fact the population, but not the very value of ${}^eE_F$.

Thus, there are at present no independent measurements performed on pure bismuth and capable of confirming either of the values cited above for E_g.

7. HOLE SPECTRUM

Since the holes are located at a point T that has high symmetry, it is much easier to treat them theoretically than the electrons. The reason is that, owing to the symmetry, certain matrix elements that describe the interaction between the bands turn out to be rigorously equal to zero. In addition, at the point T all the distances between the bands are quite large, so that it becomes possible to use methods such as the orthogonal-plane-wave or augmented-plane-wave methods. However, as already noted in Sec. a of Ch. 2, the known population of this type describe the Fermi surface quite poorly, and call for substantial corrections.

Golin[16] has advanced the hypothesis that the relative positions of the bands must be altered in such a way that the hole parameters calculated using the theoretical ma-

[5] The opposite conclusion reached by Vecchi *et al.*[21] is based on the fact that they used for comparison values of H_n measured with much lower accuracy than in[54]. The difference indicated in Fig. 19 did not exceed in this case the measurement errors.

trix elements coincide with the experimental measurements. This method of fitting leads to two doubtful results: First, some of the levels must be shifted by ~1 eV and this, taking into account the calculation accuracy, is excessive and makes the entire calculation meaningless. Second, the level closest to the valence band turns out to be at a distance ~0.2 eV, which contradicts the optical investigations, as already noted in Sec. a of Ch. 2.

Some conclusions concerning the band structure can be drawn from the experimentally obtained estimates of the deviation of the hole spectrum from parabolic. The starting point can be here the fact that the hole Fermi surface is elongated along the trigonal axis, and the corresponding masses differ by one order of magnitude. Therefore, in analogy with the case of electrons it can be assumed that Cohen's model holds for the holes, i.e., near the extremum of the valence band, in a direction perpendicular to the C_3 axis, the spectrum is described by the two-band model with a gap ${}^hE_g$, and is quadratic along C_3. Strictly speaking, this assumption is refuted by the large value, 4.26, of the g-factor of the hole at $\mathbf{H} \parallel C_3$ (Sec. b of Ch. 5); a value $g_3 > 4$ was measured also in[20], where ESR of the holes was observed. In the two-band model $g = 2$, as is obtained for holes on the basis of the deformation model.[27] But the band arrangement calculated by Golin (see Fig. 3) and the calculation[20] of the nonparabolicity of the spectrum based on this arrangement show that Cohen's model is a good approximation.

Using the spectrum (3) and assuming ${}^hE/{}^hE_g \ll 1$, we easily calculate the following quantities:

$$\left.\begin{aligned} &\frac{S_3}{S_1} = 1 + \frac{3}{8}\frac{{}^hE}{{}^hE_g}, \\ &m_3^* = m_{30}^*\left(1 + 2\frac{{}^hE}{{}^hE_g}\right), \\ &m_1^* = m_{10}^*\left(1 + \frac{5}{4}\frac{{}^hE}{{}^hE_g}\right); \end{aligned}\right\} \qquad (26)$$

m_{10}^* and m_{30}^* are the effective masses at the extremum of the valence band at $\mathbf{H} \parallel C_1$ and $\mathbf{H} \parallel C_3$, respectively. Using the experimental ratio $S_1/m_1^*/S_3/m_3^* = 1.003 \pm 0.005$ (see the end of Ch. 3) and ${}^hE_F \approx 12$ meV (Sec. b of Ch. 5), we obtain the estimate ${}^hE_g \gtrsim 600$ meV. An analogous value ${}^hE_g \approx 0.55 \pm 0.25$ eV can be obtained by using the formula for m_1^* and the value of ${}^hE_{g\,eff}$ from Sec. b of Ch. 5.

Verdun and Drew,[20] analyzing the results of measurements of the cyclotron resonance at the frequency ~10^{12} Hz in fields 50–100 kOe, reached the conclusion that ${}^hE_g = 0.21$ eV. Their calculation is based on a comparison of the effective mass in strong fields, which increases because of the increase of ${}^hE_F$ (see Sec. b, Ch. 5), with the same mass at $H \to 0$. In their analysis, however, they used the obsolescent value $m_1^*(H \to 0) = 0.203\, m_e$ from[41], and not the more accurate $m_1^* = 0.212\, m_e$ (see Table III). Since we are dealing with small changes of this value with increasing field, this difference has led to a seemingly larger nonparabolicity of the hole spectrum and to a strongly undervalued ${}^hE_g$. In fact, the experiment agrees fairly well with the large value of ${}^hE_g$ (Fig. 20). Thus, the results of[20] must be revised. We note incidentally that according to the calculation of[20] the use of Golin's matrix element[16] results in an even larger nonparabolicity of the holes.

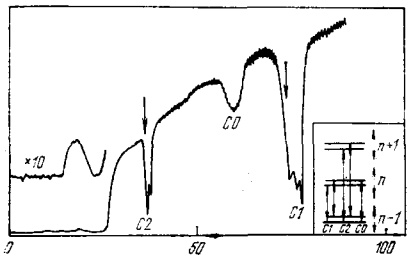

FIG. 20. Coefficient of transition of a wave with $\lambda = 311$ μm through a bismuth sample 4.3 mm thick at $T = 4.3$ K vs. the magnetic field in the Faraday configuration.[20] $\mathbf{C}_3 \perp \mathbf{H}$, the angle between $\mathbf{H}$ and $\mathbf{N}$ is $-2.5°$, and $\mathbf{H} \parallel C_2$. The arrows over the minima $C1$ and $C2$ indicate the positions of the hole cyclotron resonance calculated from the parameters obtained in Sec. b of Ch. 5.

We have considered so far only experiments on pure bismuth. It is possible to investigate the carriers in bismuth by studying alloys with other metals. In connection with the problem of determining the nonparabolicity of the hole spectrum, taking into account the scanty information obtained for pure bismuth, we discuss measurements made on alloys of the type Bi + Sn and Bi + Pb, in which a small addition (~0.01%) of an acceptor impurity changes the hole density by one order of magnitude. It is assumed that such a low concentration of the impurity atoms does not alter the spectrum of the bismuth, and merely shifts the Fermi level.

Alloys of this kind were used to investigate the Shubnikov–de Haas oscillations and to determine the hole mass at $\mathbf{H} \parallel C_3$ from the dependence of their amplitude on the temperature.[19,57] An increase of m_3^* was noted in both studies. However, whereas in[19] at $S_{alloy} \approx 3.1\, S_0$ (S_{alloy}, S_0—sections of Fermi surface for the alloy and for pure bismuth, respectively) we get $m_3^* = 0.093\, m_e$ Brandt *et al.*[57] obtained $m_3^* = 0.075\, m_e$ under the same conditions. Thus, the difference between these quantities is such that it hardly pays to discuss their deviation from the value $m_3^* = 0.0639\, m_e$ measured in pure bismuth. Obviously, on the basis of these measurements we cannot draw any conclusions concerning the hole spectrum, and in particular concerning the gaps between the bands, until the reason for the discrepancy between the results of identical experiments is made clear.

Bate *et al.*[19] succeeded also in measuring the ratio S_1/S_3 for alloys with different concentrations. It turned out that the anisotropies of the hole Fermi surface changes quite insignificantly. Thus, $S_1/S_3 = 3.16 \pm 0.1$ at a hole density 3.9×10^{18} cm^{-3}, which is close to the value 3.327 ± 0.0001 for pure bismuth (see Table III). Using formulas (26), we can estimate from this ${}^hE_g = 170$–740 meV, which in any case does not contradict the estimate given above for ${}^eE_g$. Thus, measurements with alloys have so far not yielded reliable results. The values ${}^hE_g \lesssim 200$ cited in[19,57] and obtained on the

basis of these experiments are in fact not substantiated. Measurements on pure bismuth point to ${}^{h}E_{g} \gtrsim 500$ meV.

8. CONCLUSION

Let us summarize the results and attempt to indicate some prospects of further research. As follows from the foregoing, bismuth is one of the most investigated metals, both theoretically and experimentally. High accuracy was attained in the determination of the Fermi surface and of the effective masses, and in the establishment of the character of the energy spectrum of the electrons and holes. The electron spectrum of bismuth can be regarded as known with an accuracy perfectly adequate for many applications.

However, the problem of describing the electrons can still not be regarded as completely solved. This problem is made exceedingly complicated by the fact that experiment can yield information on the electron spectrum at the bottom of the band only if simplified theoretical models are used, and the situation is such that it is difficult to reconcile the results of various experiments (see Fig. 6). As a result, even the value of such an important parameter as the gap between the bands cannot be regarded as finally established.

Let us point out some experiments that can add to our knowledge of the electronic properties of bismuth. These can be, for example, measurements in a quantizing field at higher accuracy and a larger range of fields. As shown by the measurements of the quantum oscillations at low temperatures,[37] it is possible to increase the accuracy in these experiments by one or two orders of magnitude, especially in the field region >70–100 kOe, which becomes more and more accessible to investigations.

The potential of magneto-optical investigations can likewise not be regarded as fully exhausted. Although utmost accuracy and resolution have already been attained here, much can be gained from experiment in fields $H>150$ kOe, at which infrared measurements have not yet been performed. In particular, one can expect the appearance of resonant splitting as a result of spin splitting of the Landau levels or the deviation from the two-band model, the relative magnitude of which increases in proportion to $\sqrt{H}$. It would be of great interest to observe resonant transitions for heavy electrons at $\mathbf{H} \parallel C_2$. Since in strong fields the Fermi level drops considerably, electrons situated practically at the bottom of the band will take part in such transitions. No less interesting, and easier to realize in practice, is the measurement of cyclotron resonance of light electrons at frequencies $\sim (0.5–1)\times 10^{13}$ Hz, when one should observe in fields ~10 kOe transitions from the zeroth to the first Landau level, whose energy can be determined with sufficient accuracy.

As to the refining the hole spectrum, the most reliable way in our opinion is a further increase of the accuracy with which the Fermi surface is measured. It is possible that in magneto-optical investigations at energies $\gtrsim 0.6$ eV and fields $\gtrsim 100$ kOe it will become possible to observe the fine structure of the resonance-absorption lines. Such an experiment would undoubtedly add considerably to our knowledge of the energy spectrum of bismuth.

An extensive field is research on the bismuth spectrum by investigating alloys with other metals or under pressure, and by extrapolating the obtained parameters to zero impurity concentration. In Ch. 6 we have considered some of these experiments, but refrained from a more detailed discussion for a number of reasons.

First, impurities and pressure lead primarily to a decrease in the relaxation time and a sharp reduction in the measurement accuracy, which turns out to be much worse than in pure bismuth. Second, despite the large number of investigations in this field, they remain fragmentary to a considerable degree, since what is investigated mainly is the dc conductivity, and resonance methods have not been performed systematically heretofore. Third, the results of various investigations frequently contradict one another, as was shown in Ch. 7.

Finally, in our opinion, the most interesting of these investigations is the study of the changes produced in the spectrum by an impurity that leads to a change in the carrier density (Bi+Sn), or to the appearance of a semiconducting phase (Bi+Sb alloys or under pressure) and the extent to which the observed phenomena can be described sufficiently well on the basis of simple and frequently intuitive considerations. It is obvious that such research can be successful only if the spectrum of pure bismuth is known beforehand. Therefore further investigations of pure bismuth, particularly under conditions previously not employed in experiment, remain a pressing problem.

[1]P. Kapitza, Proc. Roy. Soc. **A119**, 401 (1928).
[2]W. Y. de Haas and P. M. van Alphen, Proc. Acad. Sci. Amsterdam **33**, 1106 (1930).
[3]L. Schubnikov and W. Y. de Haas, Comm. Phys. Lab. Univ. Leiden **207a**, **207c**, **207d**, **210a** (1930).
[4]B. A. Green and B. S. Chandrasekhar, Phys. Rev. Lett. **11**, 331 (1963).
[5]J. K. Galt, W. A. Yager, F. R. Merritt, B. B. Cetlin, and H. W. Dail, Phys. Rev. **100**, 748 (1955).
[6]S. J. Buchsbaum and J. K. Galt, Phys. Fluids **4**, 1514 (1961).
[7]M. S. Khaĭkin, Usp. Fiz. Nauk **96**, 409 (1968) [Sov. Phys. Usp. **11**, 785 (1969)].
[8]D. H. Reneker, Phys. Rev. **115**, 303 (1959).
[9]A. A. Abrikosov and L. A. Fal'kovskiĭ, Zh. Eksp. Teor. Fiz. **43**, 1089 (1962) [Sov. Phys. JETP **16**, 769 (1963)].
[10]L. A. Fal'kovskiĭ, Usp. Fiz. Nauk **94**, 3 (1968) [Sov. Phys. Usp. **11**, 1 (1968)].
[11]W. S. Boyle and G. E. Smith, Progr. Semicond. **7**, 1 (1963).
[12]V. S. Edelman, Adv. Phys. **25**, 555 (1976).
[13]S. Mase, J. Phys. Soc. Japan **13**, 434 (1958).
[14]L. G. Ferreira, J. Phys. and Chem. Sol. **28**, 1891 (1967).
[15]L. G. Ferreira, *ibid.* **29**, 387 (1968).
[16]S. Golin, Phys. Rev. **166**, 643 (1968).
[17]G. E. Smith, G. A. Baraff, and J. H. Rowell, *ibid.* **A135**, 1118 (1964).
[18]P. Y. Wang and A. L. Lin, *ibid.* **B2**, 2978 (1970).
[19]R. T. Bate, N. G. Einspruch, and P. J. May, Jr., *ibid.* **186**, 599 (1969).
[20]H. R. Verdun and H. D. Drew, *ibid.* **B14**, 1370 (1976).
[21]M. P. Vecchi, J. R. Pereira, and M. S. Dresselhaus, *ibid.* **B14**, 298 (1976).

[22]L. Esaki, L. L. Chang, P. J. Stiles, D. F. O'kane, and N. Wiser, *ibid.* **167**, 637 (1968).
[23]Y. Sawatari and M. Arai, J. Phys. Soc. Japan **28**, 360 (1970).
[24]H. T. Chu, N. K. Eib, and P. N. Henriksen, Phys. Rev. **B12**, 518 (1975).
[25]M. H. Cohen, L. M. Falicov, and S. Golin, IBM J. Res. and Develop. **8**, 215 (1964).
[26]L. A. Fal'kovskiĭ and G. S. Razina, Zh. Eksp. Teor. Fiz. **49**, 265 (1965) [Sov. Phys. JETP **22**, 187 (1966)].
[27]L. A. Fal'kovskiĭ, *ibid.*, 609 [423].
[28]A. A. Abrikosov, Zh. Eksp. Teor. Fiz. **65**, 2063 (1973) [Sov. Phys. JETP **38**, 1031 (1974)].
[29]B. Lax and J. G. Mavroides, in: Advances in Solid State Physics, Ed. F. Seitz and D. Turnball, v. 11, N.Y., Academic Press, 1960, p. 261.
[30]M. H. Cohen and E. I. Blount, Phil. Mag. **5**, 115 (1960).
[31]G. A. Baraff, Phys. Rev. **A157**, 86 (1969).
[32]M. H. Cohen, *ibid.* **121**, 387 (1961).
[33]A. A. Abrikosov, J. Low Temp. Phys. **8**, 315 (1972).
[34]S. D. Beneslavkiĭ and L. A. Fal'kovskiĭ, Fiz. Tverd. Tela (Leningrad) **15**, 1360 (1973) [Sov. Phys. Solid State **15**, 923 (1973)].
[35]J. W. McClure and K. H. Choi, Sol. State Comm. **21**, 1015 (1977).
[36]I. M. Lifshitz, M. Ya. Azbel', and M. I. Kaganov, Élektronnaya teoriya metallov (Electron Theory of Metals), Nauka, 1971.
[37]V. S. Édel'man, Zh. Eksp. Teor. Fiz. **64**, 1734 (1973) [Sov. Phys. JETP **37**, 875 (1973)].
[38]F. M. Müller, Phys. Rev. **148**, 636 (1966).
[39]R. Herrman, S. Hess, and H. U. Müller, Phys. Stat. Sol. **48**, K151 (1971).
[40]A. P. Korolyuk, Zh. Eksp. Teor. Fiz. **49**, 1009 (1965) [Sov. Phys. JETP **22**, 701 (1966)].
[41]V. S. Édel'man and M. S. Khaĭkin, *ibid.*, 107 [77].
[42]R. J. Dinger and A. W. Lowson, Phys. Rev. **137**, 5215 (1973).
[43]S. M. Cheremisin, V. S. Édel'man, and M. S. Khaĭkin, Zh. Eksp. Teor. Fiz. **61**, 1112 (1971) [Sov. Phys. JETP **34**, 594 (1972)].
[44]G. E. Smith, L. C. Hebel, and S. J. Buchsbaum, Phys. Rev. **129**, 154 (1963).
[45]V. S. Édel'man, A. P. Garevskiĭ, and V. Ya. Demikhovskiĭ, Fiz. Tverd. Tela (Leningrad) **16**, 3739 (1974) [Sov. Phys. Solid State **16**, 2435 (1974)].
[46]V. S. Édel'man, Usp. Fiz. Nauk **102**, 55 (1970) [Sov. Phys. Usp. **13**, 576 (1971)].
[47]V. P. Naberezhnykh, D. E. Zherebchevskiĭ, and V. L. Mel'nik, Zh. Eksp. Teor. Fiz. **63**, 169 (1972) [Sov. Phys. JETP **36**, 89 (1973)].
[48]L. M. Falicov and P. J. Lin, Phys. Rev. **141**, 562 (1966).
[49]R. D. Brown, R. L. Hartman, and S. H. Koenig, *ibid.* **172**, 598 (1968).
[50]V. S. Tsoĭ, Zh. Eksp. Teor. Fiz. **68**, 1849 (1975) [Sov. Phys. JETP **41**, 927 (1975)].
[51]N. B. Brandt, V. A. Yastrebova, and Ya. G. Ponomarev, Fiz. Tverd. Tela (Leningrad) **16**, 102 (1974) [Sov. Phys. Solid State **16**, 59 (1974)].
[52]M. S. Khaĭkin, L. A. Fal'kovskiĭ, V. S. Édel'man, and R. T. Mina, Zh. Eksp. Teor. Fiz. **45**, 1704 (1963) [Sov. Phys. JETP **18**, 1167 (1964)].
[53]V. S. Édel'man, Zh. Eksp. Teor. Fiz. **54**, 1726 (1968) [Sov. Phys. JETP **27**, 927 (1968)].
[54]V. S. Édel'man, Zh. Eksp. Teor. Fiz. **68**, 257 (1975) [Sov. Phys. JETP **41**, 125 (1975)].
[55]S. H. Koenig, A. A. Lopez, D. B. Smith, and J. L. Yarnell, Phys. Rev. Lett. **20**, 48 (1968).
[56]M. S. Khaĭkin and V. S. Édel'man, Zh. Eksp. Teor. Fiz. **49**, 1695 (1965) [Sov. Phys. JETP **22**, 1159 (1966)].
[57]N. B. Brandt, R. Muller, and Ya. G. Ponomarev, Zh. Eksp. Teor. Fiz. **71**, 2268 (1976) [Sov. Phys. **44**, 1196 (1976)].
[58]J. F. Koch and J. D. Jensen, Phys. Rev. **184**, 643 (1969).
[59]M. Wanner, R. E. Doezema, and V. S. Strom, *ibid.* **B12**, 2883 (1975).
[60]S. Takaoka, H. Kawamura, K. Murase, and S. Takano, *ibid.* **B13**, 1428 (1976).
[61]A. B. Golik, A. P. Korolyuk, V. I. Beletskiĭ, and V. I. Khotkevich, Zh. Eksp. Teor. Fiz. **71**, 330 (1976) [Sov. Phys. JETP **44**, 172 (1976)].
[62]A. P. Volodin, M. S. Khaĭkin, and V. S. Édel'man, Zh. Eksp. Teor. Fiz. **65**, 2105 (1973) [Sov. Phys. JETP **38**, 1052 (1974)].
[63]W. S. Boyle and A. D. Brailsford, Phys. Rev. **120**, 1943 (1960).
[64]B. Lax, K. J. Button, H. J. Zeiger, and L. M. Roth, *ibid.* **102**, 715 (1956).
[65]V. D. Kulakovskiĭ and V. D. Egorov, Fiz. Tverd. Tela (Leningrad) **15**, 2053 (1973) [Sov. Phys. Solid State **15**, 1507 (1974)].
[66]R. N. Brown, J. G. Mavroides, and B. Lax, Phys. Rev. **129**, 2055 (1963).
[67]M. Maltz and M. S. Dresselhaus, *ibid.* **B2**, 2877 (1970).
[68]M. P. Vecchi and M. S. Dresselhaus, *ibid.* **B9**, 3257 (1974).
[69]P. A. Wolf, J. Phys. and Chem. Sol. **25**, 1057 (1964).
[70]M. P. Vecchi and M. S. Dresselhaus, Phys. Rev. **B10**, 77 (1974).
[71]N. B. Brandt, E. A. Svistova, and G. Kh. Tabieva, Pis'ma Zh. Eksp. Teor. Fiz. **27**, No. 4 (1966).
[72]G. E. Smith and G. A. Williams, IBM J. Res. and Develop. **8**, 276 (1964).
[73]S. Takano and H. Kawamura, J. Phys. Soc. Japan **28**, 348 (1970).
[74]V. S. Édel'man, Pis'ma Zh. Eksp. Teor. Fiz. **18**, 236 (1973) [JETP Lett. **18**, 140 (1973)].
[75]V. Strom, A. Kamgar, and J. F. Koch, Phys. Rev. **B7**, 2435 (1973).

Translated by J. G. Adashko